Day-ahead Optimal Dispatch Model for Coupled System Considering Ladder-type Ramping Rate and Flexible Spinning Reserve of Thermal Power Units

Longjie Yang, Niancheng Zhou, *Member*, *IEEE*, Guiping Zhou, Yuan Chi, *Member*, *IEEE*, Ning Chen, *Member*, *IEEE*, Lei Wang, Qianggang Wang, *Member*, *IEEE*, and Dongfeng Chang

***Abstract*—In northern China, thermal power units (TPUs) are important in improving the penetration level of renewable energy. In such areas, the potentials of coordinated dispatch of renewable energy sources (RESs) and TPUs can be better realized, if RESs and TPUs connected to the power grid at the same point of common coupling (PCC) are dispatched as a coupled system. Firstly, the definition of the coupled system is introduced, followed by an analysis on its characteristics. Secondly, based on the operation characteristics of deep peak regulation (DPR) of TPUs in the coupled system, the constraint of the ladder-type ramping rate applicable for day-ahead dispatch is proposed, and the corresponding flexible spinning reserve constraint is further established. Then, considering these constraints and peak regulation ancillary services, a day-ahead optimal dispatch model of the coupled system is established. Finally, the operational characteristics and advantages of the coupled system are analyzed in several case studies based on a real-world power grid in Liaoning province, China. The numerical results show that the coupled system can further improve the economic benefits of RESs and TPUs under the existing policies.**

***Index Terms*—Coupled system, ladder-type ramping rate, flexible spinning reserve, day-ahead optimal dispatch, deep peak regulation, peak regulation ancillary services.**

NOMENCLATURE

A. Indices and Sets

k	Index of renewable energy sources (RESs) from 1 to K
l	Index of branch from 1 to L
n	Index of thermal power units (TPUs) from 1 to N
t	Index of time periods from 1 to T
P_n^{RPR}, P_n^{DPR}, $P_n^{\mathrm{DPRO1_{w/o}}}$, $P_n^{\mathrm{DPRO2_{w/o}}}$	Output intervals of the n^{th} TPU in regular peak regulation (RPR), deep peak regulation (DPR), the first stage of DPR without oil ($\mathrm{DPRO1_{w/o}}$), and the second stage of DPR without oil ($\mathrm{DPRO2_{w/o}}$) states

B. Decision Variables

$\alpha_{n,t}$	Start-stop status of the n^{th} TPU in the t^{th} period (1: start-up, 0: shutdown)
μ_t^{TH}	Average load rate of units started in the t^{th} period
F^{OB}	Comprehensive operation benefit of coupled system in a day
$F_{k,t}^{\mathrm{RB}}$	Generation benefit of the k^{th} RES in the t^{th} period
F_t^{PC}	Cost of purchasing reserve services from upper power grid in the t^{th} period
$F_{n,t}^{\mathrm{GB}}$, $F_{n,t}^{\mathrm{OC}}$, $F_{n,t}^{\mathrm{SC}}$, $F_{n,t}^{\mathrm{EC}}$, $F_{n,t}^{\mathrm{RC}}$	Generation benefit, operation cost, start-up cost, environmental cost, and flexible reserve cost of the n^{th} TPU in the t^{th} period
$F_{n,t}^{\mathrm{RCU}}$, $F_{n,t}^{\mathrm{RCD}}$	Plus and minus flexible reserve costs of the n^{th} TPU in the t^{th} period
$f_{n,t}^{\mathrm{U}}$, $f_{n,t}^{\mathrm{D}}$	Upward and downward flexible reserves provided by the n^{th} TPU in the t^{th} period
$L_{n,t}$	Rotor cracking cycle of the n^{th} TPU in the t^{th} period
$P_{n,t}^{\mathrm{TH}}$	Output of the n^{th} TPU in the t^{th} period

Manuscript received: December 24, 2021; revised: March 24, 2022; accepted: June 17, 2022. Date of CrossCheck: June 17, 2022. Date of online publication: July 15, 2022.

This work was supported in part by the National Key Research and Development Program of China (No. 2019YFB1505400).

L. Yang, N. Zhou, Y. Chi (corresponding author), and Q. Wang are with the State Key Laboratory of Power Transmission Equipment and System Security and New Technology, Chongqing University, Chongqing 400044, China (e-mail: 20191101333@cqu. edu. cn; cee_nczhou@cqu. edu. cn; chiyuanee@cqu. edu. cn; qianggang1987@cqu.edu.cn).

G. Zhou and L. Wang are with State Grid Liaoning Electric Power Company Limited, Shenyang 110006, China (e-mail: 18900911559@163.com; alonwang@sina.com).

N. Chen is with State Key Laboratory of Operation and Control of Renewable Energy & Storage Systems (China Electric Power Research Institute), Nanjing 210003, China (e-mail: chen_ning@epri.sgcc.com.cn).

D. Chang is with Xi'an Thermal Power Research Institute Company Limited, Xi'an 710054, China (e-mail: changdongfeng@tpri.com.cn).

DOI: 10.35833/MPCE.2021.000801

P_t^{PRSU}, P_t^{PRSD} Upward and downward flexible reserve power purchased from upper power grid in the t^{th} period

$P_{k,t}^{\mathrm{RE}}$ Output power of the k^{th} RES in the t^{th} period

$P_{l,t}^{\mathrm{br}}$ Transmission power of branch l in the t^{th} period

C. Parameters

ΔT Dispatch time scale

μ_1^{TH}, μ_2^{TH} The maximum average load rates of units started in the first and second phases of peak regulation ancillary services

ω_n^{DPR} Operation loss coefficient of the n^{th} TPU in DPR state

$\lambda_{k,t}$ Proportion of curtailed output power to its predicted output power of the k^{th} RES in the t^{th} period

λ_k' Proportion of total curtailed output power to its total predicted output power of the k^{th} RES in a day

a_n, b_n, c_n Coefficients of consumption characteristic function of the n^{th} TPU

C^{coal} Coal price

C_n^{THP} Purchasing cost of the n^{th} TPU

C_0^{TH} Generation price of TPUs

C_1^{TH}, C_2^{TH} Compensation prices for TPUs participating in the first and second phases of peak regulation ancillary services

C_1^{FRU}, C_2^{FRU}, C_3^{FRU}, C_1^{FRD}, C_2^{FRD}, C_3^{FRD} Plus and minus flexible reserve prices of TPU in RPR, $\mathrm{DPRO1}_{\mathrm{w/o}}$, and $\mathrm{DPRO2}_{\mathrm{w/o}}$

C^{PRSU}, C^{PRSD} Prices of purchasing plus and minus spinning reserve services

$P_{n,\min}^{\mathrm{TH}}$, $P_{n,\max}^{\mathrm{TH}}$ The minimum and maximum outputs of the n^{th} TPU

$P_{n,\min}^{\mathrm{RPR}}$, $P_{n,\min}^{\mathrm{DPRO1}_{\mathrm{w/o}}}$, $P_{n,\min}^{\mathrm{DPRO2}_{\mathrm{w/o}}}$ The minimum output of the n^{th} TPU during RPR, $\mathrm{DPRO1}_{\mathrm{w/o}}$, and $\mathrm{DPRO2}_{\mathrm{w/o}}$

$P_{k,t}^{\mathrm{RE,pre}}$ Predicted output power of the k^{th} RES in the t^{th} period

P_t^{SFU}, P_t^{SFD} Plus and minus power demands of coupled system in the t^{th} period

P_t^{G} Power demand of upper power grid for coupled system in the t^{th} period

$P_l^{\mathrm{br,max}}$ Transmission power limit

$R_{1,n}$, $R_{2,n}$, $R_{3,n}$ Ramping rates of the n^{th} TPU in RPR, $\mathrm{DPRO1}_{\mathrm{w/o}}$, and $\mathrm{DPRO2}_{\mathrm{w/o}}$

I. Introduction

ALONG with the submission of the Paris Agreement on national independent emission reduction contributions, actively addressing climate change has become a global consensus [1], [2]. The establishment of an energy system centered on a high proportion of renewable energy has become an important trend in the world's energy development and a core element of the energy revolution promoted by many countries [3], [4]. However, the inherent intermittency and volatility of wind and photovoltaic (PV) power generation compromise the flexibility of power systems [5]. Specifically, in northern China where flexible and adjustable power sources such as hydropower and combustion engines are limited, thermal power units (TPUs) are one of the few devices that can provide flexibility to the system [6], [7]. The power system will face more serious challenges to achieve a high level of renewable energy consumption in such areas.

In order to enhance the level of clean energy utilization and power system operation efficiency, the ancillary service market and wind-thermal bundled system are being widely explored and studied [7]-[12]. In China, for example, improving the level of renewable energy consumption is mainly through measures such as peak regulation ancillary service market and TPU flexibility reformation [12], [13]. In studies on peak regulation ancillary services, [14] describes the primary rules of the deep peak regulation (DPR) market in the Northeast China Grid and analyzes the advantages and characteristics of the DPR market. Reference [15] analyzes the economics of the joint operation of thermal power plants with additional energy storage equipment in the case of high penetration level of wind power. In [16], the bilateral coordination of wind and TPUs in the DPR market is studied. Current related research focuses on the impact of policies, dispatching strategies, and single device on the participation of thermal power plants in peak regulation ancillary services, while the form of various devices participating in peak regulation ancillary services simultaneously has not been studied. For example, renewable energy sources (RESs) and TPUs coupled at the same point of common coupling (PCC) are common in power systems; when they are regarded as a coupled system, they can jointly participate in peak regulation ancillary services. This approach can further improve the overall control performance and economic efficiency of the system, and promote the coordinated development of RESs and TPUs. However, the research on the situation or dispatch approach of RESs and TPUs coupled at the same PCC remains little.

As the main peak regulation resources participating in peak regulation ancillary services, the DPR of TPUs has been widely implemented and studied [17]-[21]. In [17], to promote the accommodation of RESs, a stochastic unit commitment model considering DPR and optimal transmission switching is established. A comprehensive optimal unit commitment model between wind power curtailment and the DPR degree of TPU is proposed in [18], to give an economic alternative between the scheme of wind power curtailment and DPR of TPU. Considering the economy of the DPR stage of TPUs, a unit combination optimization model with the joint constraint of "DPR and coal consumption" is established in [19]. These studies on DPR use conventional ramping rate constraints of TPUs. However, when TPUs participate in peak regulation ancillary services, as the unit load decreases, the boiler combustion and hydrodynamic conditions

deteriorate, so do the operation efficiency and the operation stability of TPUs [22], [23]. Hence, the ramping rate of TPUs will decrease with the reduction of unit load. The conventional ramping rate constraints of TPUs cannot accurately reflect the operation characteristics of TPUs during DPR. Therefore, a ladder-type ramping rate constraint is proposed in [23] for the first time. But the constraint is too complicated for the establishment and simulation of the dispatch model of TPUs with DPR capacity.

Besides, when RESs and TPUs form a coupled system at the same PCC, the uncertainty of RES generation will be preferentially smoothed by TPUs in the coupled system. Therefore, there are higher requirements imposed on the flexible regulation capability of TPUs after system coupling. Reference [24] proposes a clustered unit commitment formulation to accurately model flexibility requirements, which solves the overestimation issue inherent to the classic clustered unit commitment. In [25], a modified flexible ramping product model is proposed to address the massive penetration of intermittent RESs in modern power systems. This model further enhances real-time market flexibility by procuring additional ramp-up capacity from the day-ahead market spinning reserve services. However, none of the above studies consider the issue of decreasing ramping capacity of TPUs as the unit load decreases during DPR. Therefore, [26] proposes a mixed-integer linear programming model for the dynamic ramping of units that allows intraperiod changes. As a result, operation reserves are better allocated and the flexibility of units is managed more efficiently. Nonetheless, the study does not consider the reduction in regulation capacity of TPUs during DPR, nor does it take into account the impact of spinning reserve in the current period on spinning reserve in the preceding and following periods. This may lead to a mismatch between the actual spinning reserve provided by the TPUs and the demand of the system.

Therefore, to address the problem of accommodating a higher proportion of RESs in regions with limited flexible and controllable power sources, a coupled system formed by RESs and TPUs at the same PCC is studied in this paper. Furthermore, the equipment parameters and operation data of a local power grid in Liaoning province, China are used for simulation and analysis. The technical contributions of this paper are summarized as follows.

1) A ladder-type ramping rate constraint applicable for day-ahead dispatch is proposed. This constraint improves the ramping rate constraint in [23] based on the operation characteristics of TPUs under different dispatch time scales. This constraint can more simply and effectively reflect the ramping capacity of TPUs with DPR capacity in day-ahead dispatch, and address the overestimation issue of the conventional ramping rate constraint for TPUs during DPR.

2) A flexible spinning reserve constraint of TPUs is proposed according to the ladder-type ramping characteristics of TPUs with the DPR capacity. The constraint not only considers the decreasing ramping capacity of TPUs as the unit load decreases during DPR, but also considers the impact of spinning reserve in the current period on spinning reserve in the preceding and following periods. It addresses the issue of conventional approach that overestimates the ability of TPU to provide spinning reserve during peak regulation, especially during DPR.

3) A flexible reserve cost model for the coupled system is proposed considering different costs of the spinning reserve under different peak regulation states of TPUs. Furthermore, a more accurate day-ahead optimal dispatch model for the coupled system than that in [23] is established by combining the ladder-type ramping rate constraint, flexible spinning reserve constraint, and flexible reserve cost model proposed in this paper. It can accurately reflect the operation characteristics of the coupled system in day-ahead dispatch, and provides a new model for the joint operation of RESs and TPUs for regions with limited flexible and controllable power sources.

II. Basics of Coupled System

For regions with limited flexible and controllable power sources, it is prevalent for RESs and TPUs to be connected to the upper power grid at the same PCC. In this situation, both physical distance and electrical connections of RESs and TPUs are close. Hence, the RESs and TPUs can be coupled as a unified dispatching and operation entity. It is important to note that the coupling relationship mentioned in this paper is different from that in the integrated energy system (IES) and multi-energy system (MES). The coupling relationship in the IES and MES refers to the coupling between different energies, such as electricity-heat-gas coupling. This coupling relationship improves the overall energy efficiency and flexibility of the system through the conversion, storage, and transference between different energies [27]-[29]. While the coupling relationship in this paper refers to the electric coupling of RESs and TPUs that are connected to the upper power grid at the same PCC with the following advantages: ① enhanced coordination and better dispatching capability; ② easy implementation and convenient extension as a module.

Therefore, in this paper, an RES-penetrated power system with RESs and TPUs coupled at the same PCC is defined as a coupled system, and its typical structure is shown in Fig. 1.

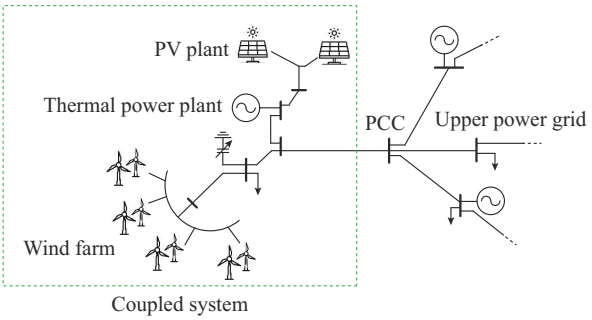

Fig. 1. Typical structure of coupled system.

As a typical way to couple RESs and TPUs, the coupled system receives dispatching instructions from the upper power grid through the substation at the PCC, and then dispatches the output of each power source in the system according to dispatching instructions. The coupled system mainly has the following characteristics.

1) As a unified dispatching entity, the coupled system can be easily integrated into the existing dispatch system.

2) The coupled system has better controllability of power output. It can reduce the peak-valley difference and improve the ability to support the stability of a power system.

3) The coupled system is prevalent. In the power grid of Liaoning, China, for example, the installed capacity of RESs and TPUs coupled at the same PCC accounts for more than 42%.

4) Capacity configuration, cooperative control, optimal operation, and other related technologies of the coupled system can be popularized and applied to the multi-source power system with multiple PCCs. Similarly, the current research approaches related to the multi-source power system, such as those in [30] and [31], can also provide references for studying the coupled system.

Compared with the independent operation of RESs and TPUs, the coupled system can give full play to the complementary characteristics of RESs and TPUs. By compensating the volatility of RES output through the rapid regulation of TPUs in the coupled system, the smooth and controllable power of the PCC can be realized. In addition, the coupled system formed by RESs and TPUs at the same PCC can participate in the peak regulation ancillary service market as a dispatch entity. It can participate in power market transactions with smoother and more controllable output. This approach can improve the comprehensive economic benefit and promote the coordinated development of RESs and TPUs.

However, the maximum ramping rate and flexible spinning reserves that TPUs can provide at different time of the day are closely related to their current state of peak regulation. Conventional operation constraints of TPUs fail to reflect this relationship. Therefore, before establishing the day-ahead optimal dispatch model of the coupled system, it is necessary to redefine the operation constraints of TPUs that consider the DPR state.

III. Improved Practical Operation Constraints of TPUs

The operation states of the TPU consist of regular peak regulation (RPR) and DPR. DPR can be divided into DPR without oil ($DPRO_{w/o}$) and DPR with oil ($DPRO_{w}$) [32]. According to the relationship between unit load and ramping rate, $DPRO_{w/o}$ can be further divided into the first stage of $DPRO_{w/o}$ ($DPRO1_{w/o}$) and the second stage of $DPRO_{w/o}$ ($DPRO2_{w/o}$). The diagram of peak regulation process of TPUs is shown in Fig. 2.

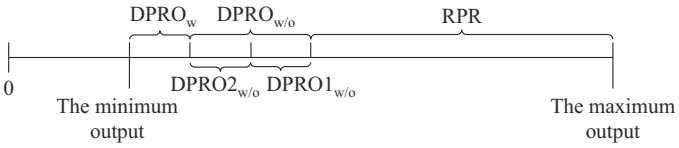

Fig. 2. Diagram of peak regulation process of TPUs.

At present, the operation of TPUs is very unstable during the $DPRO_{w}$ and exposed to accidents such as boiler extinguishing, water circulation stagnation or backflow [22], [23]. Thus, $DPRO_{w}$ is avoided in an engineering practice. It is reasonable and practical to ignore the case of TPUs operating in the $DPRO_{w}$ in this study.

A. Ladder-type Ramping Rate Constraint of TPUs

According to the test report provided by Xi'an Thermal Power Research Institute Company Limited about the operation test on a N660-25/600/600 turbine developed and produced by Siemens, the ramping rates of TPUs vary in different peak regulation states. The relationship between unit loads and ramping rates is shown in Fig. 3.

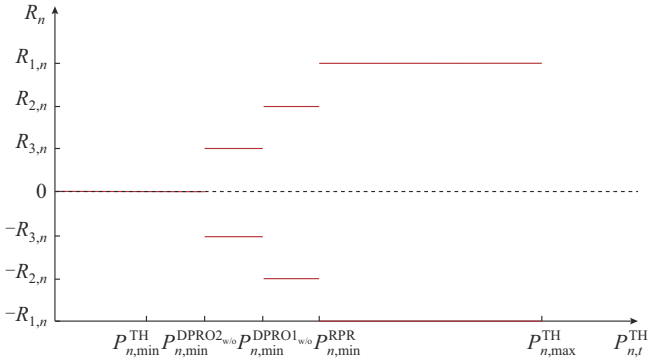

Fig. 3. Relationship between unit loads and ramping rates.

According to this test report, the conclusion on the trend of the maximum ramping rate variation of units operating in different peak regulation states shown in this test report is applicable to all units. However, the range of each peak regulation state and the maximum ramping rates that can be provided within the corresponding peak regulation states of units will be different due to various factors.

For a given TPU, the feasible region of its output in dispatch period t is mainly affected by ΔT. The TPU studied in this paper is taken as an example. For different ΔT, the feasible region of the output of the n^{th} TPU in the t^{th} period $P_{n,t}^{\text{TH}}$ is shown in Fig. 4. It should be noted that TPU operating in DPR can be directly shut down, while when TPU is started, it cannot directly enter in DPR.

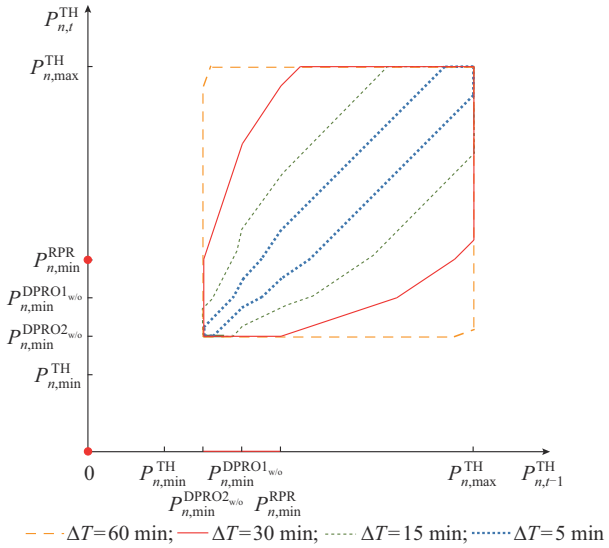

Fig. 4. Feasible regions of $P_{n,t}^{\text{TH}}$ for different ΔT.

From Fig. 4, it can be observed that the feasible regions of $P_{n,t}^{\mathrm{TH}}$ vary significantly for different ΔT. Since ΔT of day-ahead dispatch is generally 30 min and above, the ramping rate constraint of TPUs is investigated in this paper based on the feasible regions of $P_{n,t}^{\mathrm{TH}}$ for $\Delta T \geq 30$ min in Fig. 4.

Moreover, without considering the start-stop state of the TPU, it can be observed from Fig. 4 that the feasible region of $P_{n,t}^{\mathrm{TH}}$ is a convex set when ΔT is a definite value greater than or equal to 30 min, while it is a nonconvex set when $\Delta T < 30$ min. So, the feasible regions of $P_{n,t}^{\mathrm{TH}}$ for $\Delta T \geq 30$ min can be directly expressed by the boundary constraints of the convex set, without the need to discuss the ramping rate constraint of the TPU in subsections as (1)-(9) in [23]. Furthermore, by considering the start-stop state of the TPU based on the feasible regions of $P_{n,t}^{\mathrm{TH}}$ for $\Delta T \geq 30$ min, the expression of the ladder-type ramping rate constraint applicable for day-ahead dispatch ($\Delta T \geq 30$ min) can be obtained as (1).

$$
\begin{cases}
P_{n,t}^{\mathrm{TH}} - P_{n,t-1}^{\mathrm{TH}} \leq \alpha_{n,t-1} R_{1,n} \Delta T + \left(\alpha_{n,t} - \alpha_{n,t-1}\right) P_{n,\min}^{\mathrm{RPR}} \\
P_{n,t-1}^{\mathrm{TH}} - P_{n,t}^{\mathrm{TH}} \leq \alpha_{n,t} R_{1,n} \Delta T + \left(\alpha_{n,t-1} - \alpha_{n,t}\right) P_{n,\min}^{\mathrm{RPR}} \\
\dfrac{R_{2,n}}{R_{1,n}} P_{n,t}^{\mathrm{TH}} - P_{n,t-1}^{\mathrm{TH}} \leq \alpha_{n,t-1} \left[R_{2,n} \Delta T - \left(1 - \dfrac{R_{2,n}}{R_{1,n}}\right) P_{n,\min}^{\mathrm{RPR}} \right] + \\
\qquad \left(\alpha_{n,t} - \alpha_{n,t-1}\right) \dfrac{R_{2,n}}{R_{1,n}} P_{n,\min}^{\mathrm{RPR}} \\
\dfrac{R_{2,n}}{R_{1,n}} P_{n,t-1}^{\mathrm{TH}} - P_{n,t}^{\mathrm{TH}} \leq \alpha_{n,t} \left[R_{2,n} \Delta T - \left(1 - \dfrac{R_{2,n}}{R_{1,n}}\right) P_{n,\min}^{\mathrm{RPR}} \right] + \\
\qquad \left(\alpha_{n,t-1} - \alpha_{n,t}\right) \dfrac{R_{2,n}}{R_{1,n}} P_{n,\min}^{\mathrm{RPR}} \\
\dfrac{R_{3,n}}{R_{1,n}} P_{n,t}^{\mathrm{TH}} - P_{n,t-1}^{\mathrm{TH}} \leq \alpha_{n,t-1} \left[R_{3,n} \Delta T - \left(\dfrac{R_{3,n}}{R_{2,n}} - \dfrac{R_{3,n}}{R_{1,n}} \right) P_{n,\min}^{\mathrm{RPR}} \right] - \\
\qquad \alpha_{n,t-1} \left(1 - \dfrac{R_{3,n}}{R_{2,n}}\right) P_{n,\min}^{\mathrm{DPRO1_{w/o}}} + \left(\alpha_{n,t} - \alpha_{n,t-1}\right) \dfrac{R_{3,n}}{R_{1,n}} P_{n,\min}^{\mathrm{RPR}} \\
\dfrac{R_{3,n}}{R_{1,n}} P_{n,t-1}^{\mathrm{TH}} - P_{n,t}^{\mathrm{TH}} \leq \alpha_{n,t} \left[R_{3,n} \Delta T - \left(\dfrac{R_{3,n}}{R_{2,n}} - \dfrac{R_{3,n}}{R_{1,n}} \right) P_{n,\min}^{\mathrm{RPR}} \right] - \\
\qquad \alpha_{n,t} \left(1 - \dfrac{R_{3,n}}{R_{2,n}}\right) P_{n,\min}^{\mathrm{DPRO1_{w/o}}} + \left(\alpha_{n,t-1} - \alpha_{n,t}\right) \dfrac{R_{3,n}}{R_{1,n}} P_{n,\min}^{\mathrm{RPR}} \\
P_{n,t}^{\mathrm{TH}} \geq \left(\alpha_{n,t} - \alpha_{n,t-1}\right) P_{n,\min}^{\mathrm{RPR}} \\
\alpha_{n,t} P_{n,\min}^{\mathrm{DPRO2_{w/o}}} \leq P_{n,t}^{\mathrm{TH}} \leq \alpha_{n,t} P_{n,\max}^{\mathrm{TH}}
\end{cases}
\tag{1}
$$

As observed from (1), all feasible regions of $P_{n,t}^{\mathrm{TH}}$ satisfies (1) for different time scale cases with $\Delta T \geq 30$ min, and only part of the constraints in (1) becomes inactive constraints due to different ΔT. Moreover, the ladder-type ramping rate constraint of TPUs still preserves the conventional ramping rate constraint (as the first two inequity equations) of TPUs. Therefore, (1) greatly simplifies the ladder-type ramping rate constraint proposed in [23], and can reflect the ramping capacity of TPUs with DPR capacity in day-ahead dispatch.

B. Flexible Spinning Reserve Constraints of TPUs

Since the ramping capacity of TPUs decreases as the unit load decreases during DPR, it is important to accurately compute the reserve that TPUs can provide for each time period. The output of the n^{th} TPU during the RPR in a certain dispatch period is shown in Fig. 5. In Fig. 5, A_0, B_0, and C_0 denote the output power of the TPU at $t-1$, t, and $t+1$, respectively; $\overline{A_1A_2}$, $\overline{B_1B_2}$, and $\overline{C_1C_2}$ denote the minimum spinning reserve power required to be supplied by the n^{th} TPU at $t-1$, t, and $t+1$, respectively; and the slopes of the red line segments denote the maximum ramping rate of the TPU.

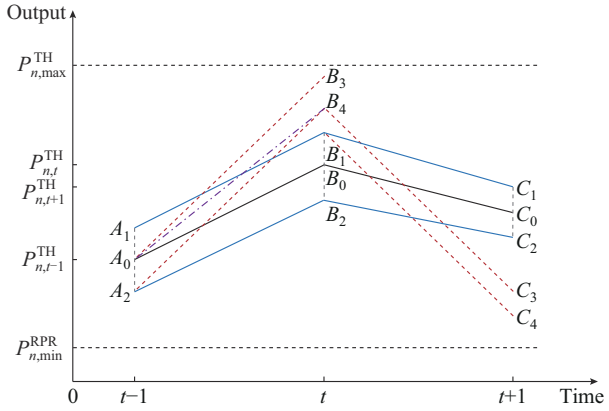

Fig. 5. Output of the n^{th} TPU during RPR in a certain dispatch period.

The maximum possible increase in the output power of the TPU within ΔT is from point A_0 to point B_3, when the flexible reserve of the TPU at $t-1$ is not considered. However, since the TPU needs to provide the minimum downward flexible reserve $\overline{A_0A_2}$ at $t-1$, in practice the maximum output power that can be increased by the TPU in ΔT is from point A_0 to point B_4. That is, the maximum upward flexible reserve that the TPU can provide at t is $\overline{B_0B_4}$. In the same way, when the TPU provides the upward flexible reserve $\overline{B_0B_1}$ at t, the maximum downward flexible reserve that the TPU can provide at $t+1$ is $\overline{C_0C_4}$. When the TPU provides the upward flexible reserve $\overline{B_0B_4}$ at t, the maximum downward flexible reserve that the TPU can provide at $t+1$ is $\overline{C_0C_3}$. It is clear that the maximum flexible reserve that a TPU can provide in each period is affected not only by the ramping rate and output range of TPUs, but also by the flexible reserve that has been provided in the previous period. Therefore, during the RPR, the flexible reserve that can be provided for each dispatch period of the TPU can be expressed as:

$$
\begin{cases}
f_{n,t}^{\mathrm{U}} \geq 0 \\
f_{n,t}^{\mathrm{U}} \leq P_{n,\max}^{\mathrm{TH}} - P_{n,t}^{\mathrm{TH}} \\
f_{n,t}^{\mathrm{U}} \leq R_{1,n} \Delta T - \left(P_{n,t}^{\mathrm{TH}} - P_{n,t-1}^{\mathrm{TH}}\right) - f_{n,t-1}^{\mathrm{D}} \\
f_{n,t}^{\mathrm{D}} \geq 0 \\
f_{n,t}^{\mathrm{D}} \leq P_{n,t}^{\mathrm{TH}} - P_{n,\min}^{\mathrm{RPR}} \\
f_{n,t}^{\mathrm{D}} \leq R_{1,n} \Delta T + \left(P_{n,t}^{\mathrm{TH}} - P_{n,t-1}^{\mathrm{TH}}\right) - f_{n,t-1}^{\mathrm{U}}
\end{cases}
\tag{2}
$$

In addition to operating in a fixed peak regulation state, the operation states of the TPU may also change from one

peak regulation state to another in a dispatch period. When the state of peak regulation changes, the ramping rate of the TPU also changes, which affects the spinning reserve that the TPU can provide. Therefore, according to Fig. 4, Fig. 5, (1), and (2), the maximum flexible reserve that a TPU can provide in different situations can be deduced. Finally, the flexible spinning reserve constraints of TPUs can be derived as:

$$\begin{cases} f_{n,t}^{\mathrm{U}} \ge 0 \\ f_{n,t}^{\mathrm{U}} \le P_{n,\max}^{\mathrm{TH}} - P_{n,t}^{\mathrm{TH}} \\ f_{n,t}^{\mathrm{U}} \le 0 \quad \forall \alpha_{n,t}\alpha_{n,t-1} \ne 1 \\ f_{n,t}^{\mathrm{U}} \le R_{1,n}\Delta T - \left(P_{n,t}^{\mathrm{TH}} - P_{n,t-1}^{\mathrm{TH}}\right) - f_{n,t-1}^{\mathrm{D}} \quad \forall \alpha_{n,t}\alpha_{n,t-1} = 1 \\ f_{n,t}^{\mathrm{U}} \le R_{1,n}\Delta T - \left(P_{n,t}^{\mathrm{TH}} - \dfrac{R_{1,n}}{R_{2,n}} P_{n,t-1}^{\mathrm{TH}}\right) + \\ \qquad \left(1 - \dfrac{R_{1,n}}{R_{2,n}}\right) P_{n,\min}^{\mathrm{RPR}} - f_{n,t-1}^{\mathrm{D}} \quad \forall \alpha_{n,t}\alpha_{n,t-1} = 1 \\ f_{n,t}^{\mathrm{U}} \le R_{1,n}\Delta T - \left(P_{n,t}^{\mathrm{TH}} - \dfrac{R_{1,n}}{R_{3,n}} P_{n,t-1}^{\mathrm{TH}}\right) + \left(1 - \dfrac{R_{1,n}}{R_{2,n}}\right) P_{n,\min}^{\mathrm{RPR}} + \\ \qquad \left(\dfrac{R_{1,n}}{R_{2,n}} - \dfrac{R_{1,n}}{R_{3,n}}\right) P_{n,\min}^{\mathrm{DPRO1_{w/o}}} - f_{n,t-1}^{\mathrm{D}} \quad \forall \alpha_{n,t}\alpha_{n,t-1} = 1 \end{cases} \tag{3}$$

$$\begin{cases} f_{n,t}^{\mathrm{D}} \ge 0 \\ f_{n,t}^{\mathrm{D}} \le P_{n,t}^{\mathrm{TH}} - P_{n,\min}^{\mathrm{DPRO2_{w/o}}} \quad \forall \alpha_{n,t} = 1 \\ f_{n,t}^{\mathrm{D}} \le 0 \quad \forall \alpha_{n,t}\alpha_{n,t-1} \ne 1 \\ f_{n,t}^{\mathrm{D}} \le R_{1,n}\Delta T + \left(P_{n,t}^{\mathrm{TH}} - P_{n,t-1}^{\mathrm{TH}}\right) - f_{n,t-1}^{\mathrm{U}} \quad \forall \alpha_{n,t}\alpha_{n,t-1} = 1 \\ f_{n,t}^{\mathrm{D}} \le R_{2,n}\Delta T + \left(P_{n,t}^{\mathrm{TH}} - \dfrac{R_{2,n}}{R_{1,n}} P_{n,t-1}^{\mathrm{TH}}\right) - \\ \qquad \left(1 - \dfrac{R_{2,n}}{R_{1,n}}\right) P_{n,\min}^{\mathrm{RPR}} - f_{n,t-1}^{\mathrm{U}} \quad \forall \alpha_{n,t}\alpha_{n,t-1} = 1 \\ f_{n,t}^{\mathrm{D}} \le R_{3,n}\Delta T + \left(P_{n,t}^{\mathrm{TH}} - \dfrac{R_{3,n}}{R_{1,n}} P_{n,t-1}^{\mathrm{TH}}\right) + \left(\dfrac{R_{3,n}}{R_{1,n}} - \dfrac{R_{3,n}}{R_{2,n}}\right) P_{n,\min}^{\mathrm{RPR}} - \\ \qquad \left(1 - \dfrac{R_{3,n}}{R_{2,n}}\right) P_{n,\min}^{\mathrm{DPRO1_{w/o}}} - f_{n,t-1}^{\mathrm{U}} \quad \forall \alpha_{n,t}\alpha_{n,t-1} = 1 \end{cases} \tag{4}$$

As can be observed from (3) and (4), compared with the conventional spinning reserve constraints, the flexible spinning reserve constraints of TPUs consider both the variation of ramping capacity with different peak regulation states and the impact of spinning reserve in the preceding and following periods on spinning reserve in the current period. These constraints can avoid the problem of overestimating the ability of TPUs to provide spinning reserve.

The rest of the operation constraints for TPUs are the same as those for conventional operation of TPUs and can be found in [33].

IV. Day-ahead Optimal Dispatch Model of Coupled System

Taking the coupled system formed by RESs and TPUs at the same PCC as the research object, this paper establishes the day-ahead optimal dispatch model of the coupled system. The model aims at maximizing the comprehensive operation benefit of the coupled system in a single day with the operation constraints of TPUs proposed in this paper.

A. Objective Function

The comprehensive operation benefit of the coupled system in a day mainly consists of two parts, i. e., generation benefit and operation cost, which can be expressed as:

$$F^{\mathrm{OB}} = \max \sum_{t=1}^{T} \left[\sum_{k=1}^{K} F_{k,t}^{\mathrm{RB}} + \sum_{n=1}^{N} \left(F_{n,t}^{\mathrm{GB}} - F_{n,t}^{\mathrm{OC}} - F_{n,t}^{\mathrm{SC}} - F_{n,t}^{\mathrm{EC}} - F_{n,t}^{\mathrm{RC}} \right) - F_{t}^{\mathrm{PC}} \right] \tag{5}$$

In (5), $F_{k,t}^{\mathrm{RB}}$, $F_{n,t}^{\mathrm{SC}}$, and $F_{n,t}^{\mathrm{EC}}$ can be found in [23].

1) Generation Benefit of TPUs

According to the operation regulations of the peak regulation ancillary service market, thermal power plants are compensated for ancillary services when the average load rate of TPUs started in the unit statistical period is less than or equal to the peak regulation compensation benchmark [34]. Therefore, the generation benefit of TPUs in the coupled system can be expressed as:

$$F_{n,t}^{\mathrm{GB}} = \begin{cases} C_0^{\mathrm{TH}} P_{\mathrm{n},t}^{\mathrm{TH}} \Delta T & \mu_1^{\mathrm{TH}} < \mu_t^{\mathrm{TH}} \le 1 \\ C_0^{\mathrm{TH}} P_{\mathrm{n},t}^{\mathrm{TH}} \Delta T + C_1^{\mathrm{TH}} \left(\mu_1^{\mathrm{TH}} \alpha_{n,t} P_{n,\max}^{\mathrm{TH}} - P_{\mathrm{n},t}^{\mathrm{TH}} \right) \Delta T & \mu_2^{\mathrm{TH}} < \mu_t^{\mathrm{TH}} \le \mu_1^{\mathrm{TH}} \\ C_0^{\mathrm{TH}} P_{\mathrm{n},t}^{\mathrm{TH}} \Delta T + C_2^{\mathrm{TH}} \left(\mu_1^{\mathrm{TH}} \alpha_{n,t} P_{n,\max}^{\mathrm{TH}} - P_{\mathrm{n},t}^{\mathrm{TH}} \right) \Delta T & 0 \le \mu_t^{\mathrm{TH}} \le \mu_2^{\mathrm{TH}} \end{cases} \tag{6}$$

$$\mu_t^{\mathrm{TH}} = \sum_{n=1}^{N} P_{n,t}^{\mathrm{TH}} \Big/ \sum_{n=1}^{N} \left(\alpha_{n,t} P_{n,\max}^{\mathrm{TH}} \right) \tag{7}$$

2) Operation Cost of TPUs

When the TPU is in an RPR state, its operation cost is mainly the operation coal consumption cost. When the TPU is in a DPR state, its operation cost will incur the operation loss cost in addition to the operation coal consumption cost. Therefore, the operation cost of the TPU can be obtained as:

$$F_{n,t}^{\mathrm{OC}} = \begin{cases} \left(a_n \left(P_{n,t}^{\mathrm{TH}} \right)^2 + b_n P_{n,t}^{\mathrm{TH}} + c_n \right) C^{\mathrm{coal}} \Delta T & P_{n,t}^{\mathrm{TH}} \in P_n^{\mathrm{RPR}} \\ \left[\left(a_n \left(P_{n,t}^{\mathrm{TH}} \right)^2 + b_n P_{n,t}^{\mathrm{TH}} + c_n \right) C^{\mathrm{coal}} + \omega_n^{\mathrm{DPR}} C_n^{\mathrm{THP}} \Big/ \left(2L_{n,t} \right) \right] \Delta T & P_{n,t}^{\mathrm{TH}} \in P_n^{\mathrm{DPR}} \\ 0 & P_{n,t}^{\mathrm{TH}} = 0 \end{cases} \tag{8}$$

3) Flexible Reserve Cost of TPUs

The TPUs need to provide flexible reserves to deal with the fluctuation of RESs and load in the coupled system, which leads to the flexible reserve cost. The smaller the output of TPUs, the greater the operation loss of TPUs, and the higher the flexible reserve cost will be. Therefore, the flexible reserve cost of TPUs can be obtained as:

$$F_{n,t}^{\mathrm{RC}} = F_{n,t}^{\mathrm{RCU}} + F_{n,t}^{\mathrm{RCD}} \tag{9}$$

$$F_{n,t}^{\mathrm{RCU}}=\begin{cases}C_1^{\mathrm{FRU}} f_{n,t}^{\mathrm{U}}\Delta T & \forall f_{n,t}^{\mathrm{U}}+P_{n,t}^{\mathrm{TH}}\in P_n^{\mathrm{RPR}}, P_{n,t}^{\mathrm{TH}}\in P_n^{\mathrm{RPR}}\\ \left[C_2^{\mathrm{FRU}}\left(P_{n,\min}^{\mathrm{RPR}}-P_{n,t}^{\mathrm{TH}}\right)+C_1^{\mathrm{FRU}}\left(f_{n,t}^{\mathrm{U}}+P_{n,t}^{\mathrm{TH}}-P_{n,\min}^{\mathrm{RPR}}\right)\right]\Delta T & \forall f_{n,t}^{\mathrm{U}}+P_{n,t}^{\mathrm{TH}}\in P_n^{\mathrm{RPR}}, P_{n,t}^{\mathrm{TH}}\in P_n^{\mathrm{DPRO1_{w/o}}}\\ C_2^{\mathrm{FRU}} f_{n,t}^{\mathrm{U}}\Delta T & \forall f_{n,t}^{\mathrm{U}}+P_{n,t}^{\mathrm{TH}}\in P_n^{\mathrm{DPRO1_{w/o}}}, P_{n,t}^{\mathrm{TH}}\in P_n^{\mathrm{DPRO1_{w/o}}}\\ \left[C_3^{\mathrm{FRU}}\left(P_{n,\min}^{\mathrm{DPRO1_{w/o}}}-P_{n,t}^{\mathrm{TH}}\right)+C_2^{\mathrm{FRU}}\left(P_{n,\min}^{\mathrm{RPR}}-P_{n,\min}^{\mathrm{DPRO1_{w/o}}}\right)+C_1^{\mathrm{FRU}}\left(f_{n,t}^{\mathrm{U}}+P_{n,t}^{\mathrm{TH}}-P_{n,\min}^{\mathrm{RPR}}\right)\right]\Delta T & \forall f_{n,t}^{\mathrm{U}}+P_{n,t}^{\mathrm{TH}}\in P_n^{\mathrm{RPR}}, P_{n,t}^{\mathrm{TH}}\in P_n^{\mathrm{DPRO2_{w/o}}}\\ \left[C_3^{\mathrm{FRU}}\left(P_{n,\min}^{\mathrm{DPRO1_{w/o}}}-P_{n,t}^{\mathrm{TH}}\right)+C_2^{\mathrm{FRU}}\left(f_{n,t}^{\mathrm{U}}+P_{n,t}^{\mathrm{TH}}-P_{n,\min}^{\mathrm{DPRO1_{w/o}}}\right)\right]\Delta T & \forall f_{n,t}^{\mathrm{U}}+P_{n,t}^{\mathrm{TH}}\in P_n^{\mathrm{DPRO1_{w/o}}}, P_{n,t}^{\mathrm{TH}}\in P_n^{\mathrm{DPRO2_{w/o}}}\\ C_3^{\mathrm{FRU}} f_{n,t}^{\mathrm{U}}\Delta T & \forall f_{n,t}^{\mathrm{U}}+P_{n,t}^{\mathrm{TH}}\in P_n^{\mathrm{DPRO2_{w/o}}}, P_{n,t}^{\mathrm{TH}}\in P_n^{\mathrm{DPRO2_{w/o}}}\\ 0 & \text{others}\end{cases} \tag{10}$$

$$F_{n,t}^{\mathrm{RCD}}=\begin{cases}C_1^{\mathrm{FRD}} f_{n,t}^{\mathrm{D}}\Delta T & \forall P_{n,t}^{\mathrm{TH}}-f_{n,t}^{\mathrm{D}}\in P_n^{\mathrm{RPR}}, P_{n,t}^{\mathrm{TH}}\in P_n^{\mathrm{RPR}}\\ \left[C_1^{\mathrm{FRD}}\left(P_{n,t}^{\mathrm{TH}}-P_{n,\min}^{\mathrm{RPR}}\right)+C_2^{\mathrm{FRD}}\left(f_{n,t}^{\mathrm{D}}-P_{n,t}^{\mathrm{TH}}+P_{n,\min}^{\mathrm{RPR}}\right)\right]\Delta T & \forall P_{n,t}^{\mathrm{TH}}-f_{n,t}^{\mathrm{D}}\in P_n^{\mathrm{DPRO1_{w/o}}}, P_{n,t}^{\mathrm{TH}}\in P_n^{\mathrm{RPR}}\\ \left[C_1^{\mathrm{FRD}}\left(P_{n,t}^{\mathrm{TH}}-P_{n,\min}^{\mathrm{RPR}}\right)+C_2^{\mathrm{FRD}}\left(P_{n,\min}^{\mathrm{RPR}}-P_{n,\min}^{\mathrm{DPRO1_{w/o}}}\right)+C_3^{\mathrm{FRD}}\left(f_{n,t}^{\mathrm{D}}-P_{n,t}^{\mathrm{TH}}+P_{n,\min}^{\mathrm{DPRO1_{w/o}}}\right)\right]\Delta T & \forall P_{n,t}^{\mathrm{TH}}-f_{n,t}^{\mathrm{D}}\in P_n^{\mathrm{DPRO2_{w/o}}}, P_{n,t}^{\mathrm{TH}}\in P_n^{\mathrm{RPR}}\\ C_2^{\mathrm{FRD}} f_{n,t}^{\mathrm{D}}\Delta T & \forall P_{n,t}^{\mathrm{TH}}-f_{n,t}^{\mathrm{D}}\in P_n^{\mathrm{DPRO1_{w/o}}}, P_{n,t}^{\mathrm{TH}}\in P_n^{\mathrm{DPRO1_{w/o}}}\\ \left[C_2^{\mathrm{FRD}}\left(P_{n,t}^{\mathrm{TH}}-P_{n,\min}^{\mathrm{DPRO1_{w/o}}}\right)+C_3^{\mathrm{FRD}}\left(f_{n,t}^{\mathrm{D}}-P_{n,t}^{\mathrm{TH}}+P_{n,\min}^{\mathrm{DPRO1_{w/o}}}\right)\right]\Delta T & \forall P_{n,t}^{\mathrm{TH}}-f_{n,t}^{\mathrm{D}}\in P_n^{\mathrm{DPRO2_{w/o}}}, P_{n,t}^{\mathrm{TH}}\in P_n^{\mathrm{DPRO1_{w/o}}}\\ C_3^{\mathrm{FRD}} f_{n,t}^{\mathrm{D}}\Delta T & \forall P_{n,t}^{\mathrm{TH}}-f_{n,t}^{\mathrm{D}}\in P_n^{\mathrm{DPRO2_{w/o}}}, P_{n,t}^{\mathrm{TH}}\in P_n^{\mathrm{DPRO2_{w/o}}}\\ 0 & \text{others}\end{cases} \tag{11}$$

As can be observed from (10) and (11), the flexible reserve cost model is more complex than the conventional spinning reserve cost model after considering different costs of the spinning reserve under different peak regulation states of TPUs. It can accurately reflect the spinning reserve cost of TPUs in the coupled system.

4) Cost of Purchasing Spinning Reserve Services

Spinning reserve services need to be purchased from the upper power grid when TPUs in the coupled system cannot provide sufficient flexible reserves. The cost of purchasing spinning reserve services can be expressed as:

$$F_t^{\mathrm{PC}}=C^{\mathrm{PRSU}}P_t^{\mathrm{PRSU}}\Delta T+C^{\mathrm{PRSD}}P_t^{\mathrm{PRSD}}\Delta T \tag{12}$$

B. Constraints

The operation constraints of the coupled system include power balance constraints, RES generation constraints, flexible reserve constraints, power flow constraints, and TPU operation constraints. Among them, the TPU operation constraints have been described in Section III.

1) Power Balance Constraints

$$\sum_{n=1}^{N}P_{n,t}^{\mathrm{TH}}+\sum_{k=1}^{K}P_{k,t}^{\mathrm{RE}}=P_t^{\mathrm{G}} \tag{13}$$

2) RES Generation Constraints

The RESs in the coupled system can improve the stability and economy of the coupled system operation by actively curtailing part of the output power. However, the output power of RESs that can be curtailed in each time period and the total output power that can be curtailed in a day cannot exceed the specified values. Therefore, the RES generation constraints can be obtained as:

$$\begin{cases}P_{k,t}^{\mathrm{RE}}\geq\left(1-\lambda_{k,t}\right)P_{k,t}^{\mathrm{RE,pre}}\\ \sum_{t=1}^{T}P_{k,t}^{\mathrm{RE}}\geq\left(1-\lambda_k'\right)\sum_{t=1}^{T}P_{k,t}^{\mathrm{RE,pre}}\end{cases} \tag{14}$$

3) Flexible Reserve Constraints

When the flexible reserve provided by TPUs is sufficient, the coupled system will not have a power shortage in operation. When the flexible reserve provided by TPUs is insufficient, it will cause the coupled system to have a power shortage in operation, and then it is necessary to purchase reserve power from the upper power grid. Therefore, the flexible reserve constraints of the coupled system can be given as:

$$\begin{cases}\sum_{n=1}^{N}f_{n,t}^{\mathrm{U}}+P_t^{\mathrm{PRSD}}\geq P_t^{\mathrm{SFD}}\\ \sum_{n=1}^{N}f_{n,t}^{\mathrm{D}}+P_t^{\mathrm{PRSU}}\geq P_t^{\mathrm{SFU}}\end{cases} \tag{15}$$

4) Power Flow Constraints

The transmission power of each branch in the coupled system should not exceed its limit:

$$-P_l^{\mathrm{br,max}}\leq P_{l,t}^{\mathrm{br}}\leq P_l^{\mathrm{br,max}} \tag{16}$$

The day-ahead optimal dispatch model of the coupled system established in this paper is a complex mixed-integer nonlinear programming model. In this paper, the model is first linearized by using piecewise linearization and Big-*M* method to transform it into a mixed-integer linear programming model, and then the model is solved by using the CPLEX 12.9 solver on the MATLAB R2016b through the YALMIP toolbox. Besides, the application of more efficient solving algorithms in this model is straightforward.

V. Case Studies

A. Test System and Parameters

In this paper, a real-world local power grid in Liaoning province, China is used as an example for simulation analysis, as shown in Fig. 6, which consists of a 2×600 MW ther-

mal power plant, a 300 MW offshore wind farm, a 100 MW PV plant, and a planned 300 MW PV plant. All of them are coupled at the same PCC (point A in Fig. 6) to form a coupled system.

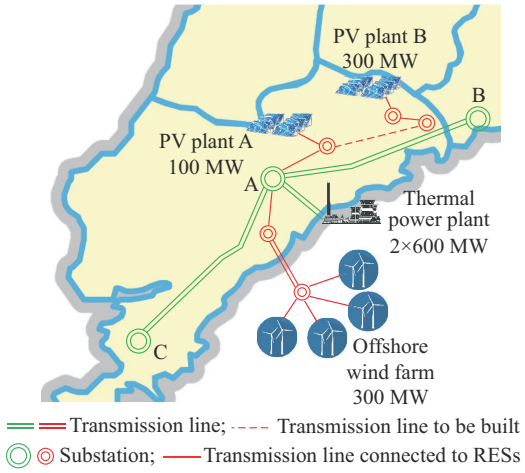

Fig. 6. Schematic diagram of a real-world local power grid in Liaoning province, China.

The operation parameters of TPUs are shown in Table I.

TABLE I
OPERATION PARAMETERS OF TPUS

Parameter	Value
Capacity (MW)	600
The minimum start-stop time (hour)	8
Start-up cost (¥)	480000
Output range of RPR (MW)	[300, 600]
Output range of $DPRO1_{w/o}$ (MW)	[240, 300]
Output range of $DPRO2_{w/o}$ (MW)	[180, 240]
Ramping rate in RPR (MW/min)	9
Ramping rate in $DPRO1_{w/o}$ (MW/min)	6
Ramping rate in $DPRO2_{w/o}$ (MW/min)	3
Flexible reserve price in RPR (¥/MW)	12
Flexible reserve price in $DPRO1_{w/o}$ (¥/MW)	15
Flexible reserve price in $DPRO2_{w/o}$ (¥/MW)	18
Generation price (¥/MW)	375
Unit construction price (¥/MW)	3464000
Coal price (¥/t)	685

According to the operation rules of the peak regulation ancillary service market, when the load factor of the thermal power plant is 40%-50% and less than 40%, the compensation prices of real-time DPR transaction of TPUs are 400 ¥/MWh and 800 ¥/MWh, respectively. The feed-in tariff of offshore wind power generation is 850 ¥/MWh, the feed-in tariff of PV power generation is 740 ¥/MWh, and the prices of purchasing plus and minus spinning reserve services are both 25 ¥/MW.

The wind and PV power prediction curves and PCC power curves for a day of this local power grid used for simulation are shown in Fig. 7. The dispatch time scale is 30 min.

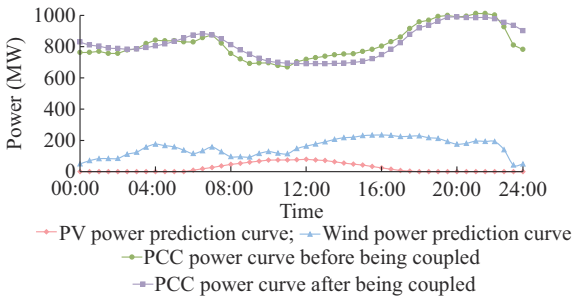

Fig. 7. Wind and PV power prediction curves and PCC power curves.

B. Comparison Study for Test System Before and After Being Coupled

When the thermal power plant, offshore wind farm, and PV plant in the local power grid operate independently, the output of the thermal power plant is regulated by the upper power grid, and the uncertainty of the output of the offshore wind farm and PV plant is also addressed by the upper power grid. In this case, the PCC power is the total output power of the thermal power plant, offshore wind farm, and PV plant, called the PCC power before being coupled. When the local power grid operates as a coupled system, it can be regulated as a whole by the upper power grid, and the uncertainty of the output of the offshore wind farm and PV plant is addressed by the thermal power plant first. In this case, the PCC power is the output power demand of the upper power grid to the coupled system, called the PCC power after being coupled. Four different scenarios are studied as follows and the numerical results are shown in Table II.

TABLE II
NUMERICAL RESULTS OF FOUR DIFFERENT SCENARIOS

Scenario	Comprehensive operation benefit (¥)	Wind power generation benefit (¥)	PV power generation benefit (¥)
1	5772629.34	3158422.35	421067.40
2	5818366.51	3158422.35	421067.40
3	5868193.85	3158422.35	421067.40
4	5916411.83	3158369.31	389815.91

Scenario	Cost of purchasing reserve services (¥)	Comprehensive benefit of TPUs (¥)	Benefit of TPUs (¥)
1	74522.17	2267661.76	6272987.50
2	125.50	2239002.26	6272987.50
3	2596.96	2291301.06	6462034.86
4	2905.08	2371131.69	6447262.10

Scenario	Operation cost (¥)	Start-up cost (¥)	Environmental cost (¥)
1	3990371.26	0	1841.80
2	3990371.26	0	1841.80
3	4128129.04	0	1841.80
4	4032462.82	0	1846.40

Scenario	Flexible reserve cost (¥)	Benefit of ancillary services (¥)	Utilization rate of renewable energy (%)
1	13112.68	497800.00	100.00
2	41772.18	497800.00	100.00
3	40762.96	686847.36	100.00
4	41821.19	656214.29	99.01

1) Scenario 1: each plant or farm operates independently, and the PCC power is the same as that before being coupled.

2) Scenario 2: all plants and farms operate as a coupled system, and the PCC power is the same as that before being coupled.

3) Scenario 3: all plants and farms operate as a coupled system, and the PCC power is the same as that after being coupled.

4) Scenario 4: all plants and farms operate as a coupled system, the PCC power is the same as that after being coupled, and the curtailment of wind and PV power is allowed.

As can be observed from Table II, the difference in the comprehensive operation benefits of scenarios 1 and 2 mainly depends on different reserve costs. In scenario 1, the uncertainty of the output of the offshore wind farm and PV plant is addressed by the upper power grid, but in scenario 2, the uncertainty is firstly addressed by the local TPUs. Because the unit price of purchasing reserve services from the upper power grid is higher than that of the flexible reserve, although the flexible reserve cost in scenarios 2 is increased by ¥28659.5 compared with scenario 1, the cost of purchasing reserve services is decreased by ¥74396.67. As a result, the comprehensive operation benefit of scenario 2 is higher than that of scenario 1.

In scenario 3, the PCC power is the output power demand of the upper power grid to the coupled system. As can be observed from Fig. 5, the PCC power after being coupled is lower than that before being coupled during DPR. Hence, the output of TPUs is lower during DPR, which leads to the increase of the operation loss of TPUs and the decrease of the flexible reserve that can be provided by TPUs. As a result, compared with scenario 2, the operation cost of TPUs is increased by ¥137757.78, the flexible reserve cost is decreased by ¥1009.22, while the cost of purchasing reserve services is increased by ¥2471.46. However, because the output of TPUs is lower during DPR, the benefit of peak regulation ancillary services is increased by ¥189047.36. Hence, the comprehensive operation benefit of scenario 3 is increased relative to scenario 2.

Scenario 4 allows appropriate wind and PV power curtailment on the basis of scenario 3. In this case, the output of TPUs is increased during RPR. Therefore, compared with scenario 3, although the benefit of peak regulation ancillary services is decreased by ¥30633.07, the TPU benefit is only decreased by ¥14772.76, and the operation cost of TPUs is decreased by ¥95666.22. As a result, compared with scenario 3, although the sum of wind and PV power generation benefits is decreased by ¥31304.53 (0.99% curtailment rate of renewable energy), the comprehensive operation benefit of the coupled system is increased by ¥48217.98 (0.82%) instead.

In summary, compared with the conventional independent operation mode, the coupled system generates more stable and controllable output. Thus, it is helpful in satisfying dispatch requirements of the upper power grid, and can obtain higher comprehensive operation benefit.

C. Sensitivity Analysis of Coupled System to Installed Capacity of RESs

In this paper, the installed capacity of PV plant is analyzed as an example. The impact of the increase in the installed capacity of wind farm is similar to the PV plant case, and both of them only affect the PCC power and the peak and valley values of RES output.

The following scenarios of increased installed capacity of PV plant are simulated, respectively.

1) Scenario A: all plants and farms operate as a coupled system, the PCC power is the same as that after being coupled, the installed capacity of PV plant increases by 100 MW, and the curtailment of wind and PV power is not considered.

2) Scenario B: all plants and farms operate as a coupled system, the PCC power is the same as that after being coupled, the installed capacity of PV plant increases by 200 MW, and the curtailment of wind and PV power is not considered.

3) Scenario C: all plants and farms operate as a coupled system, the PCC power is the same as that after being coupled, the installed capacity of PV plant increases by 300 MW, and the curtailment of wind and PV power is not considered.

4) Scenario D: all plants and farms operate as a coupled system, the PCC power is the same as that after being coupled, the installed capacity of PV plant increases by 300 MW, and the curtailment of wind and PV power is considered.

Figure 8 shows the PCC power curves considering different increase values of installed capacity of PV plant, and the simulation results of the four scenarios are shown in Table III.

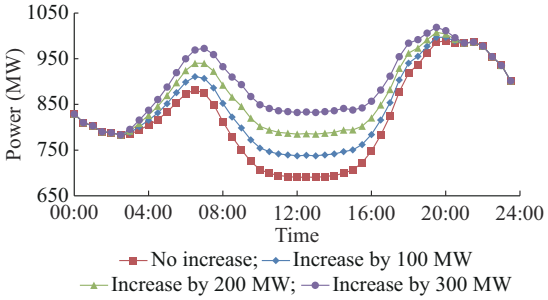

Fig. 8. PCC power curves considering different increase values of installed capacity of PV plant.

The results from scenario 3 in Table II and scenarios A, B in Table III show that with each increase by 100 MW increase in the installed capacity of PV plant, the PV power generation benefits are both increased by ¥421067.4, while the comprehensive operation benefits are increased by ¥396426.12 and ¥442082.47, respectively. It is because with the increase in installed capacity of PV plant, the output of TPUs is further reduced. Although the benefit of ancillary services is increased by ¥139841.94, the operation cost is increased by ¥161026.6 due to the TPUs maintain low output. Ultimately, the increased comprehensive operation benefit is less than the increased PV power generation benefit. When changing from scenario A to scenario B, the output of TPUs is already very low, and the output that can be further reduced is limited. As a result, both the benefit of ancillary ser-

vices and operation cost are increased more slowly. From the results, it can be observed that the benefit of ancillary services is increased by ¥84493.5, while the operation cost is only increased by ¥58161.92. Furthermore, since only limited reserve can be obtained from the low-output TPUs, the coupled system needs to purchase spinning reserve services from the upper power grid, which leads to an increase of the cost of purchasing reserve services by ¥5309.82. Finally, the increased comprehensive operation benefit is more than the increased PV power generation benefit.

TABLE III
SIMULATION RESULTS OF FOUR DIFFERENT SCENARIOS

Scenario	Comprehensive operation benefit (¥)	Wind power generation benefit (¥)	PV power generation benefit (¥)
A	6264619.97	3158422.35	842134.80
B	6706702.44	3158422.35	1263202.20
C	6784669.81	3158422.35	1684269.60
D	7194970.17	3158422.35	1660851.60
Scenario	Cost of purchasing reserve services (¥)	Comprehensive benefit of TPUs (¥)	Benefit of TPUs (¥)
A	5207.15	2269269.97	6601876.80
B	10516.97	2295594.86	6686370.30
C	8703.82	1950681.68	5775187.50
D	18118.16	2393814.38	6762773.87
Scenario	Operation cost (¥)	Start-up cost (¥)	Environmental cost (¥)
A	4289155.64	0.00	1841.80
B	4347317.56	0.00	1841.80
C	3301221.96	480000.00	1814.27
D	4324967.70	0.00	1845.24
Scenario	Flexible reserve cost (¥)	Benefit of ancillary services (¥)	Utilization rate of renewable energy (%)
A	41609.39	826689.30	100.00
B	41616.08	911182.80	100.00
C	41469.59	0.00	100.00
D	42146.55	975719.14	99.47

In addition, it can be observed in scenario C that one TPU is shut down. It is because the PV output is high during the RPR. At this time, two TPUs simultaneously operating with the minimum output will also exceed the dispatch demand of the upper power grid. Under the condition that active wind and PV power curtailment is not allowed, one TPU is forced to be shut down to ensure the dispatch demand of the upper power grid. As the operation of a single TPU cannot meet the compensation conditions of peaking auxiliary services, it cannot obtain the benefit of peak regulation ancillary services. Therefore, the above situation causes an economic loss of ¥344913.18 to the TPUs. However, due to the PV power generation benefit is increased by ¥421067.4, the comprehensive operation benefit is still increased by ¥77967.37.

In scenario D, appropriate curtailment of renewable energy during DPR can prevent TPUs from being shut down. The simulation results show that scenario D can increase the comprehensive operation benefit by ¥410300.36 (6.05%) compared with scenario C with the renewable energy curtailment rate of only 0.53%.

To sum up, when the renewable energy curtailment is not allowed, the comprehensive operation benefit of the coupled system is gradually increased with RES capacity, and the benefit growth rate first accelerates and then slows down. However, when the share of RES capacity exceeds a certain percentage, it will cause the shutdown of TPUs or curtailment of renewable energy. Therefore, in order to accommodate more renewable energy in the coupled system, the TPUs need to be further reformed.

D. Comparison Study for Proposed Model and Models in Existing Work

To further illustrate the advantages of the ladder-type ramping rate constraint, flexible spinning reserve constraints, and flexible reserve cost model proposed in this paper, the simulation is performed for scenario 3 using the constraints and model proposed in this paper and those proposed in [23], respectively. The models used are as follows and the corresponding simulation results are shown in Table IV.

1) Model 1: using the ladder-type ramping rate constraint in [23], the conventional spinning reserve cost model, and the conventional spinning reserve constraints.

2) Model 2: using the flexible spinning reserve constraints and flexible reserve cost model in this paper, and the ladder-type ramping rate constraint in [23].

3) Model 3: using the ladder-type ramping rate constraint and flexible reserve cost model in this paper, and the conventional spinning reserve constraints.

4) Model 4: using the ladder-type ramping rate constraint and flexible spinning reserve constraints in this paper, and the conventional spinning reserve cost model.

5) Model 5: using the ladder-type ramping rate constraint, flexible spinning reserve constraints, and flexible reserve cost model in this paper.

TABLE IV
SIMULATION RESULTS OF FIVE DIFFERENT MODELS

Model	Comprehensive operation benefit (¥)	Benefit of TPUs (¥)	Operation cost (¥)
1	5873493.22	6462034.86	4128129.04
2	5868193.85	6462034.86	4128129.04
3	5869246.04	6462034.86	4128129.04
4	5872390.60	6462034.86	4128129.04
5	5868193.85	6462034.86	4128129.04
Model	Flexible reserve cost (¥)	Cost of purchasing reserve services (¥)	Simulation time (s)
1	37239.32	821.23	9.12
2	40762.96	2596.96	875.05
3	41486.50	821.23	13.68
4	36365.46	2641.75	9.13
5	40762.96	2596.96	79.49

First, by comparing model 2 and model 4, it can be observed that the ladder-type ramping rate constraint proposed in this paper reduces the simulation time by about 90% compared with that in [23] without affecting the simulation results. This is because the ladder-type ramping rate constraint proposed in

this paper makes full use of the characteristics of the convex set, and reduces the number of 0-1 variables in the constraint. Therefore, the simulation time is significantly reduced.

Second, by comparing models 1, 3, 4, and 5, it can be observed that using either the conventional constraints and model or the constraints and model proposed in this paper do not have impact on the output of TPUs, but only on the spinning reserve cost of TPUs. When using the conventional constraints and model, the issues of decreasing ramping capacity and increasing spinning reserve cost of TPUs as the unit load decreases during DPR are not considered. Therefore, it would be overly optimistic to estimate the spinning reserve cost of TPUs and the cost of purchasing spinning reserve services. For example, model 3 does not consider the issue of decreasing ramping capacity of TPUs as the unit load decreases during DPR, thus it understates the spinning reserve power purchased from the upper power grid by about 68% compared with model 5. Model 4 does not consider the issue of increasing spinning reserve cost of TPUs as the unit load decreases during DPR, thus it understates the spinning reserve cost of TPUs by about 10% compared with model 5. Moreover, since the constraints and model proposed in this paper are more complex than the conventional constraints and model, the simulation time is increased by about 85% as a result.

Therefore, the ladder-type ramping rate constraint proposed in this paper can significantly reduce the simulation time while not affecting the simulation results, and the flexible spinning reserve constraints and flexible reserve cost model can more accurately portray the actual spinning reserve and spinning reserve cost of TPUs.

VI. Conclusion

This paper elaborates the definition and characteristics of the coupled system of RESs and TPUs connected to the power grid through the same PCC, proposes the ladder-type ramping rate and flexible spinning reserve constraints of TPUs applicable to day-ahead dispatch, and establishes a flexible reserve cost model. Based on these constraints and the model, a day-ahead optimal dispatch model of the coupled system is proposed. The specific conclusions are as follows.

1) The ladder-type ramping rate constraint, flexible spinning reserve constraints, and flexible reserve cost model of TPUs applicable to day-ahead dispatch are proposed. These constraints and the model sufficiently consider the operation characteristics of TPUs during DPR, and can more accurately reflect the ramping rate and the ability to provide the spinning reserve of TPUs. These constraints and the model solve the problem that the conventional constraints overestimate the ramping rate and spinning reserve cost of TPUs, and generates more realistic simulation results that are closer to the engineering practice.

2) Based on the constraints of TPUs proposed in this paper and operation regulations of peak regulation ancillary services, the day-ahead optimal dispatch model of the coupled system is established. The simulation results show that the unified dispatch and control of RESs and TPUs through the same PCC as a coupled system can further improve the operation benefit of RESs and TPUs under the existing policies. Moreover, since the uncertainty of RES generation is preferentially smoothed by TPUs within the coupled system, the output power of the coupled system is smoother and can better respond to the dispatch commands.

3) The increase of the ratio of RES capacity will increase the operation pressure of TPUs in the coupled system. In the power grid studied in this paper, when the installed capacity of RESs exceeds 35%, the coupled system will not be able to provide DPR services while completely smoothing out fluctuations of RESs. Therefore, the TPUs must be reformed to improve their flexibility, which is one of the works that will be done in the project subsequently.

The TPUs are currently being retrofitted to accommodate more RESs. After the TPU reformation of the project is completed, further detailed tests on the related performance of the TPUs will be conducted to verify the validity of the constraints and models proposed in this paper, and to establish a more accurate model for the output of the TPUs and the optimal operation of the coupled system. Moreover, the advantages of the coupled system in peak regulation and frequency regulation will also be studied in the future.

References

[1] S. Lazarou, C. Christodoulou, and V. Vita, "Global change assessment model (GCAM) considerations of the primary sources energy mix for an energetic scenario that could meet Paris agreement," in *Proceedings of 54th International Universities Power Engineering Conference*, Bucharest, Romania, Sept. 2019, pp. 1-5.

[2] A. K. Mathur and S. Singh. "Status of India's renewable energy commitments for the Paris Agreement," in *Proceedings of 2019 International Conference on Power Generation Systems and Renewable Energy Technologies*, Istanbul, Turkey, Aug. 2019, pp. 1-5.

[3] W. Wang, S. Huang, G. Zhang *et al*., "Optimal operation of an integrated electricity-heat energy system considering flexible resources dispatch for renewable integration," *Journal of Modern Power Systems and Clean Energy*, vol. 9, no. 4, pp. 699-710, Jul. 2021.

[4] Energy Research Institute, National Development and Reform Commission. (2015, May). China 2050 high renewable energy penetration scenario and roadmap study. [Online]. Available: https://www.efchina.org/Reports-zh/china-2050-high-renewable-energy-penetration-scenario-and-roadmap-study-zh

[5] J. B. Mogo and I. Kamwa, "Improved deterministic reserve allocation method for multi-area unit scheduling and dispatch under wind uncertainty," *Journal of Modern Power Systems and Clean Energy*, vol. 5, no. 13, pp. 1142-1154, Mar. 2019.

[6] G. Luo, X Zhang, S. Liu *et al*., "Demand for flexibility improvement of thermal power units and accommodation of wind power under the situation of high-proportion renewable integration–taking north Hebei as an example," *Environmental Science and Pollution Research*, vol. 26, no. 7, pp. 7033-7047, Jan. 2019.

[7] K. Xie, J. Dong, C. Singh *et al*., "Optimal capacity and type planning of generating units in a bundled wind-thermal generation system," *Applied Energy*, vol. 164, no. 1, pp. 200-210, Feb. 2016.

[8] H. Goudarzi, M. Rayati, A. Sheikhi *et al*., "A clearing mechanism for joint energy and ancillary services in non-convex markets considering high penetration of renewable energy sources," *International Journal of Electrical Power and Energy Systems*, vol. 129, no. 3, p. 106817, Jul. 2021.

[9] P. Zou, Q. Chen, Q. Xia *et al*., "Evaluating the contribution of energy storages to support large-scale renewable generation in joint energy and ancillary service markets," *IEEE Transactions on Sustainable Energy*, vol. 7, no. 2, pp. 808-818, Apr. 2016.

[10] J. Xu, F. Wang, C. Lv *et al*., "Economic-environmental equilibrium based optimal scheduling strategy towards wind-solar-thermal power generation system under limited resources," *Applied Energy*, vol. 231, no. 1, pp. 355-371, Dec. 2018.

[11] Y. Sun and J. Dong, "Selection of desirable transmission power mode for the bundled wind-thermal generation systems," *Journal of Cleaner Production*, vol. 216, no. 1, pp. 585-596, Apr. 2019.

[12] J. Hu, Q. Yan, F. Kahrl *et al*., "Evaluating the ancillary services mar-

ket for large-scale renewable energy integration in China's northeastern power grid," *Utilities Policy*, vol. 69, no. 1, p. 101179, Apr. 2021.
[13] D. Sun, K. Sun, Q. Jian *et al*., "Integrated planning of transmission network and thermal power units' flexibility reformation," in *Proceedings of 2020 IEEE/IAS Industrial and Commercial Power System Asia*, Weihai, China, Jul. 2020, pp. 593-598.
[14] H. Ma, Z. Yan, M. Li *et al*., "Benefit evaluation of the deep peak-regulation market in the northeast china grid," *CSEE Journal of Power and Energy Systems*, vol. 5, no. 4, pp. 533-544, Dec. 2019.
[15] M. Li, Y. Wang, Y. Tian *et al*., "Deep peak shaving model of fire-storage combination under high permeability wind power conditions," in *Proceedings of 2020 IEEE Student Conference on Electric Machines and Systems*, Jinan, China, Dec. 2020, pp. 674-679.
[16] F. Peng, Z. Gao, S. Hu *et al*., "Bilateral coordinated dispatch of multiple stakeholders in deep peak regulation," *IEEE Access*, vol. 8, no. 1, pp. 33151-33162, Feb. 2020.
[17] Q. An, J. Wang, G. Li *et al*., "Role of optimal transmission switching in accommodating renewable energy in deep peak regulation-enabled power systems," *Global Energy Interconnection*, vol. 3, no. 6, pp. 577-584, Dec. 2020.
[18] B. Yang, X. Cao, Z. Cai *et al*., "Unit commitment comprehensive optimal model considering the cost of wind power curtailment and deep peak regulation of thermal unit," *IEEE Access*, vol. 8, no. 1, pp. 71318-71325, Mar. 2020.
[19] D. Song, C. Wang, J. Xu *et al*., "Study on unit optimal scheduling considering the joint constraint of 'deep peak load regulation and coal consumption'," in *Proceedings of 2020 Chinese Automation Congress*, Shanghai, China, Nov. 2020, pp. 1909-1913.
[20] J. Ren, X. Ma, X. Zhang *et al*., "Joint optimal deep peak regulation of renewable-rich power system with responsive load heating storage enabled CHP and flexible thermal plants," in *Proceedings of 2020 IEEE 4th Conference on Energy Internet and Energy System Integration*, Wuhan, China, Oct. 2020, pp. 2673-2678.
[21] C. Liu, G. Chen, Y. Huang *et al*., "Determining deep peak-regulation reserve for power system with high-share of renewable energy based on virtual energy storage," in *Proceedings of 2019 IEEE Sustainable Power and Energy Conference (iSPEC)*, Beijing, China, Nov. 2019, pp. 2690-2695.
[22] Y. Wang, S. Lou, Y. Wu *et al*., "Flexible operation of retrofitted coal-fired power plants to reduce wind curtailment considering thermal energy storage," *IEEE Transactions on Power Systems*, vol. 35, no. 2, pp. 1178-1187, Mar. 2020.
[23] L. Yang, N. Zhou, B. Hu *et al*., "Optimal scheduling method for coupled system based on ladder-type ramp rate of thermal power units," *Proceedings of the CSEE*, vol. 42, no. 1, pp. 153-164, Jan. 2022.
[24] G. Morales-Espaa and D. A. Tejada-Arango. "Modeling the hidden flexibility of clustered unit commitment," *IEEE Transactions on Power Systems*, vol. 34, no. 4, pp. 3294-3296, Jul. 2019.
[25] M. Khoshjahan, P. Dehghanian, M. Moeini-Aghtaie *et al*., "Harnessing ramp capability of spinning reserve services for enhanced power grid flexibility," *IEEE Transactions on Industry Applications*, vol. 55, no. 6, pp. 7103-7112, Jun. 2019.
[26] C. M. Correa-Posada, G. Morales-Espana, P. D. Martinez *et al*., "Dynamic ramping model including intraperiod ramp-rate changes in unit commitment," *IEEE Transactions on Sustainable Energy*, vol. 8, no. 1, pp. 43-50, Jan. 2016.
[27] W. Wang, S. Huang, G. Zhang *et al*., "Optimal operation of an integrated electricity-heat energy system considering flexible resources dispatch for renewable integration," *Journal of Modern Power Systems and Clean Energy*, vol. 9, no. 4, pp. 699-710, Jul. 2021.
[28] Y. Li, H. Zhang, X. Liang *et al*., "Event-triggered-based distributed cooperative energy management for multienergy systems," *IEEE Transactions on Industrial Informatics*, vol. 15, no. 4, pp. 2008-2022, Apr. 2019.
[29] H. Zhao, B. Wang, X. Wang *et al*., "Active dynamic aggregation model for distributed integrated energy system as virtual power plant," *Journal of Modern Power Systems and Clean Energy*, vol. 8, no. 5, pp. 831-840, Sept. 2020.
[30] P. Li, Q. Wu, M. Yang *et al*., "Distributed distributionally robust dispatch for integrated transmission-distribution systems," *IEEE Transactions on Power Systems*, vol. 36, no. 2, pp. 1193-1205, Mar. 2021.
[31] Y. Li, D. W. Gao, W. Gao *et al*., "Double-mode energy management for multi-energy system via distributed dynamic event-triggered Newton-Raphson algorithm," *IEEE Transactions on Smart Grid*, vol. 11, no. 6, pp. 5339-5356, Nov. 2020.
[32] X. Zhang, M. Wang, M Wang *et al*., "A unit commitment model considering peak regulation of units for wind power integrated power system," in *Proceedings of 2020 IEEE/IAS Industrial and Commercial Power System Asia*, Weihai, China, Jul. 2020, pp. 714-719.
[33] Y. Shi, Y. Li, Y. Zhou *et al*., "Optimal scheduling for power system peak load regulation considering short-time startup and shutdown operations of thermal power unit," *International Journal of Electrical Power and Energy Systems*, vol. 131, no. 11, p. 107012, Oct. 2021.
[34] Northeast China Energy Regulatory Bureau of National Energy Administration. (2020, Dec.). Operation rules of northeast electric power auxiliary service market. [Online]. Available: http://dbj.nea.gov.cn/zwfw/zcfg/202012/t20201223_4055300.html

Longjie Yang received the B.S. and M.S. degrees in electrical engineering from Sichuan University, Chengdu, China, in 2015 and 2019, respectively. He is currently pursuing the Ph.D. degree in School of Electrical Engineering, Chongqing University, Chongqing, China. His research interests include modeling, optimization, and operation of power system.

Niancheng Zhou received the B.S., M.S., and Ph.D. degrees in electrical engineering from Chongqing University, Chongqing, China, in 1991, 1994, and 1997, respectively. He worked at Chongqing Kuayue Technology Co., Ltd., Chongqing, China, from 1997 to 2003. He is a Professor in School of Electrical Engineering, Chongqing University. From 2010 to 2011, he was a Research Fellow of Nanyang Technological University, Singapore. His research interests include analysis and operation of power system, microgrid, and power quality.

Guiping Zhou received the B.S. and M.S. degrees in electrical engineering from Dalian University of Technology, Dalian, China, in 2004 and 2007, respectively, and the Ph.D. degree in Shenyang Institute of Automation, Chinese Academy of Sciences, Shenyang, China, in 2012. He is currently a Senior Engineer with the State Grid Liaoning Electric Power Supply Co., Ltd., Shenyang, China. His research interests include application of power system automation.

Yuan Chi received the B.E. degree from Southeast University, Nanjing, China, in 2009, the M.E. degree from Chongqing University, Chongqing, China, in 2012, and the Ph.D. degree from Nanyang Technological University, Singapore, in 2021. From 2012 to 2016, he worked as an Electrical Engineer of Power System Planning consecutively with State Grid Chongqing Electric Power Research Institute, Chongqing, China, and Chongqing Economic and Technological Research Institute, Chongqing, China. He is currently working as a Research Associate with Chongqing University. His research interests include planning and resilience of power system and voltage stability.

Ning Chen received the B.S. and M.S. degrees from the Harbin Institute of Technology, Harbin, China, in 2005 and 2007, respectively, and the Ph.D. degree from Southeast University, Nanjing, China, in 2017, all in electrical engineering. He is a Professor-level Senior Engineer with the Renewable Energy Research Center, China Electric Power Research Institute, Nanjing, China. His current research interests include renewable energy grid integration, concentrating solar power plant grid integration, and power system analysis.

Lei Wang received the B.S. degree form Harbin Engineering University, Harbin, China, in 2004, the M.S. and Ph.D. degrees from Harbin Institute of Technology, Harbin, China, in 2007 and 2011, respectively. He is currently a Senior Engineer with the State Grid Liaoning Electric Power Supply Co., Ltd., Shenyang, China. His research interests include network security management, network security architecture protection design, and network and information security technology.

Qianggang Wang received the B.S. and Ph.D. degrees from Chongqing University, Chongqing, China, in 2009 and 2015, respectively. He is currently an Associate Professor with the School of Electrical Engineering, Chongqing University. He was a Research Fellow with Nanyang Technological University, Singapore, from 2015 to 2016. His research interests include analysis and operation of power system, microgrid, and power quality.

Dongfeng Chang received the B.S. degree in building environment and equipment engineering from Xi'an Jiaotong University, Xi'an, China, in 2001, and the M.S. degree in power engineering and engineering thermophysics from Xi'an Jiaotong University, in 2006. He is currently a Senior Engineer with Xi'an Thermal Power Research Institute Co., Ltd., Xi'an, China. His research interests include energy saving, emission reduction and flexibility technology of thermal power units.